

# Automatic microseismic denoising and onset detection using the synchrosqueezed continuous wavelet transform

S. Mostafa Mousavi<sup>1</sup>, Charles A. Langston<sup>1</sup>, and Stephen P. Horton<sup>1</sup>

## ABSTRACT

Typical microseismic data recorded by surface arrays are characterized by low signal-to-noise ratios (S/Ns) and highly nonstationary noise that make it difficult to detect small events. Currently, array or crosscorrelation-based approaches are used to enhance the S/N prior to processing. We have developed an alternative approach for S/N improvement and simultaneous detection of microseismic events. The proposed method is based on the synchrosqueezed continuous wavelet transform (SS-CWT) and custom thresholding of single-channel data. The SS-CWT allows for the adaptive filtering of time- and frequency-varying noise as well as offering an improvement in resolution over the conventional wavelet transform. Simultaneously, the algorithm incorporates a detection procedure that uses the thresholded wavelet coefficients and detects an arrival as a local maxima in a characteristic function. The algorithm was tested using a synthetic signal and field microseismic data, and our results have been compared with conventional denoising and detection methods. This technique can remove a large part of the noise from small-amplitudes signal and detect events as well as estimate onset time.

## INTRODUCTION

Microseismic tremors are low-amplitude events with negative earthquake magnitude, typically between -3.0 and 0.0, that correspond to brittle failure mainly attributed to the reduction in effective stress (Maxwell, 2005). Passive microseismic monitoring has been used in the mining industry for assessing safety from rockbursts and the state of stress within a mine for more than a hundred years (Mendecki, 1993), in the exploration of water-reservoir-induced

seismicity for at least five decades (Simpson et al., 1988) and in the geothermal industry (Pearson, 1981), but its application in the oil and gas industry is relatively new. However, there has been rapid growth in the application of monitoring of microseismic events induced by hydraulic fracturing and mining during the past 30 years (Maxwell, 2005; Duncan and Eisner, 2010; Shemeta and Anderson, 2010; Rosca and Maisons, 2012).

In the mining and hydrocarbon setting, microseismic signals are recorded by sensors either distributed at the surface or in monitoring borehole(s). The accuracy and precision of the inverted locations in passive monitoring depend on the signal-to-noise ratios (S/Ns) of recorded data and the spatial distribution of the receivers. Usually, downhole monitoring provides better detection due to a higher S/N; however, precise location of events might be difficult, especially in the case of a single monitoring well (Eisner et al., 2009). Unlike the accurate depth estimation, epicentral errors for microseismic events located using downhole arrays increase as a function of distance from monitoring well. On the other hand, although surface monitoring often suffers from low S/N, epicentral solutions are more precise due to the feasibility of placing receivers at multiple azimuths and offsets. However, one of the major challenges in surface monitoring remains in distinguishing noise from the signal (Eisner et al., 2010).

Accurate and reliable automatic detection and onset-time estimation is a crucial step in the processing of passive microseismic data, which is influenced by the S/N of data and can affect other attributes, such as source location determination, source mechanism determination, and hazard assessment (Maxwell et al., 2008). Hence, in the past three decades, numerous algorithms have been developed for automatic detection (including simultaneous detection and onset picking) based on energy analyses and characteristic functions (CFs; Saari, 1991; Ruud and Husebye, 1992; Earle and Shearer, 1994; Panagiotakis et al., 2008), the ratio of short-term average (STA) to long-term average (LTA; Allen, 1978; Berand and Kradolfer, 1997), polarization analyses (Vidale, 1986; Magotra et al., 1987, 1989; Jurkevici, 1988; Anderson and Nehorai, 1996;

Manuscript received by the Editor 6 November 2015; revised manuscript received 27 March 2016; published online 10 June 2016.

<sup>1</sup>University of Memphis, Center for Earthquake Research and Information (CERI), Memphis, Tennessee, USA. E-mail: smousavi@memphis.edu; clangstn@memphis.edu; shorton@memphis.edu.

© 2016 Society of Exploration Geophysicists. All rights reserved.

Amoroso et al., 2012), artificial neural networks (Dai and MacBeth, 1995, 1997; Wang and Teng, 1995; Mousset et al., 1996; Zhao and Takano, 1999; Gentili and Michelini, 2006), fuzzy logic theory (Chu and Mendel, 1994), the time-delay technique and graph theory (Taylor et al., 2011), autoregressive techniques (Maeda, 1985; Leonard and Kennett, 1999; Sleeman and van Eck, 1999; Leonard, 2000; Zhang et al., 2003), maximum likelihood methods (Christoffersson et al., 1988; Robert et al., 1989), empirical subspace detector (Barrett and Beroza, 2014), the wavelet transform (WT; Anant and Dowla, 1997; Botella et al., 2003; Simons et al., 2006; Karamzadeh et al., 2013; Bogiatzis and Ishii, 2015), PageRank (Aguilar and Beroza, 2014), higher order statistics (HOS; Yung and Ikelle, 1997; Poletto, 2000; Saragiotis et al., 2002, 2004; Küperkoch et al., 2010; Lois et al., 2013), hybrid HOS and time-frequency analyses (Saragiotis et al., 1999; Galiana-Merino et al., 2008; Tselentis et al., 2012), and hybrid HOS and polarization analysis (Nippert et al., 2010; Baillard et al., 2014; Ross and Ben-Zion, 2014). However, the presence of the seismic noise can overly affect the performance of these methods. Hence, the development of robust and accurate automatic algorithms that perform satisfactorily for general situations, which account for differences in source type, distance, noise level, and instrument response, remains a nontrivial, active field of research (Withers et al., 1998).

The automatic detection of small events can be improved through signal enhancement. Microseismic filtering is typically performed by frequency filters, which are inadequate due to the overlap in frequency content of the signal and noise. Another approach in microseismic monitoring using surface arrays is to enhance the signal using array processing techniques, such as  $f$ - $k$  analysis (Naghizadeh, 2011) or  $f$ - $x$  filtering (Bekara and van der Baan, 2009; Naghizadeh and Sacchi, 2012; Chen and Ma, 2014). However, these methods require sufficient coherency in the arrival across the array. The other filter typically used are match filters (Gibbons and Ringdal, 2006; Eisner et al., 2008), which require an a priori event with high S/N to act as a “master” or template event for the crosscorrelation with the continuous waveform.

Seismic signal and noise often have nonstationary frequency content and vary over time (MacNamara and Buland, 2004). These time varying characteristics of the frequency content have been shown to contain useful information for the study of micro earthquakes induced by hydraulic fracturing (Pettitt et al., 2009; Das and Zoback, 2011; Tary and van der Baan, 2012; Tary et al., 2013). Time-frequency representations (TFRs) can give an insight into the complex structure of a signal consisting of several components by displaying the frequency components and their amplitudes for a given time. The advantage of using a time-frequency transforms (TFTs) for the filtering, in contrast to the more traditional spectral filtering, is that it allows for noise in the same passband as the signal to be identified and excluded from the signal, so long as it is temporally separated from signal arrivals.

Two examples of seismic denoising using TFT include using the WT with a thresholding criterion by Sobolev and Lyubushin (2006) or Mousavi and Langston (2016) for the analysis of earthquake precursors, and an application of the S-transform and the customized thresholding (CT) for optimal denoising by Parolai (2009). Galiana-Merino et al. (2008) show that using the wavepacket transform in standard thresholding of seismic waveforms can result in fewer artifacts in estimating the arrival time of the denoised signal compared

with traditional discrete wavelet thresholding methods. In a more recent study, Han and van der Baan (2015) use ensemble empirical mode decomposition and adaptive thresholding for the microseismic denoising. However, these methods are either not very effective for removing high-amplitude noise of surface microseismic data without distorting emergent arrivals of the signals (Galiana-Merino et al., 2008; Parolai, 2009), or they are not fully automated and have parameters that need to be tuned manually (Han and van der Baan, 2015).

This paper introduces an automatic and adaptive algorithm for simultaneous noise reduction and detection of microseismic events based on the so-called synchrosqueezed continuous wavelet transform (SS-CWT) and CT algorithm. Synchrosqueezing is a special case of reassignment methods that aim to provide a sharpened continuous wavelet representation by applying a postprocessing reallocation of the original representation (Daubechies and Maes, 1996; Daubechies et al., 2011). It was originally developed for the continuous wavelet transform (CWT) in audio signal processing (Daubechies et al., 2011) and shown to be a powerful and promising tool for precise identification and extraction of constituent components of multicomponent signals with time-varying frequency and amplitude (Wu et al., 2011; Li and Liang, 2012; Thakur et al., 2013; Yang, 2015). Compared with conventional transforms and classical reassignment methods, synchrosqueezing is visually more informative and adaptable to a wide variety of signals (Thakur et al., 2013). Hence, it has been successfully applied to time-frequency analysis of vibration monitoring (Li and Liang, 2012), paleoclimate time series (Thakur et al., 2013), and seismic data (Herrera et al., 2014, 2015; Tary et al., 2014).

In the following sections, a brief theoretical introduction to the SS-CWT transform and wavelet denoising will be presented, as well as details of the proposed method. The algorithm will be tested on a synthetic signal contaminated with field seismic noise to study the robustness of the proposed method for the denoising. It will also be applied to a continuous record of microseismic events, in which results are compared with standard thresholding and detection methods. The comparison shows that our proposed method yields higher S/N as well as being more reliable for detection and onset time picking.

## THEORETICAL BACKGROUND

### Synchrosqueezing-continuous wavelet transform

The main assumption behind synchrosqueezing is that smearing in the TFR mainly occurs in the scale frequency axis, and it is negligible along the time axis. Hence, concentrating the time-frequency map into the most representative instantaneous frequencies will decrease the smearing, while still allowing reconstruction of the signal.

SS-CWT is performed in three steps. First, we assume that the signal  $s(t)$  is a superposition of nonstationary components that can be efficiently decomposed to time-scale “atoms” using the CWT (Herrera et al., 2014):

$$s(t) = \sum_{k=1}^K f_k(t) + \epsilon(t), \quad (1)$$

where  $s(t)$  is the recorded time series,  $f_k(t)$  represents various seismic signals corrupted by additive Gaussian noise,  $\epsilon \sim N(0, \sigma^2)$ , and  $K$  is the number of components in the signal.

The idea behind the CWT is to apply a prototype analyzing function known as the “mother wavelet” as a band-pass filter over the time series. For a given mother wavelet  $\psi$ , the CWT of  $s(t)$  at scale  $a$  and time shift  $\tau$  is given by (Grossman and Morlet, 1984; Daubechies, 1988, 1992; Heil and Walnut, 1989; Farge, 1992)

$$W_s(a, \tau) = \langle s, \psi_{a, \tau} \rangle = \int s(t) a^{-1/2} \psi^* \left( \frac{t - \tau}{a} \right) dt, \quad (2)$$

where the  $*$  is the complex conjugate,  $\langle y, \psi_{a, \tau} \rangle$  is the inner product in  $L^2(R)$ , and  $W_s$  is the coefficient representing energy of the observed signal  $s(t)$  at scale  $a$ . The mother wavelet must satisfy the admissibility condition; that is, if  $\psi$  is integrable, it has zero mean, or

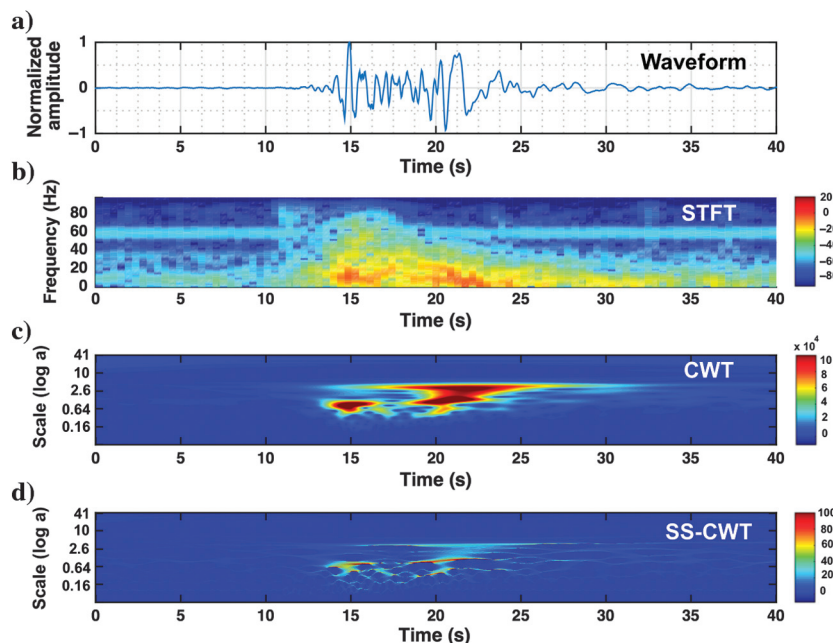
$$\int_{-\infty}^{\infty} \psi(t) dt = 0. \quad (3)$$

If the function  $s(t)$  is discrete, then equation 2 becomes a summation of the signal with the scale and normalized wavelet kernel.

The CWT is an inner product in  $L^2(R)$  (Mallat, 1999), and can be described as a series of crosscorrelation operations between the signal  $s(t)$  and several wavelets that are scaled and translated versions of the original mother wavelet  $\psi$ . The variable length of the mother wavelet leads to a more flexible trade-off between time and frequency localization compared with the short-time Fourier transform (STFT), but still, the energy is spread out in the time-scale plane, which results in a blurred TFR.

The instantaneous frequencies are ridges in the TFR (Auger et al., 2013). The CWT representation is improved by a reassignment step, squeezing the energy around the ridges (condensing the CWT coefficients at each time point along the scale axis). Hence, in the second step, an initial estimation of the instantaneous frequency  $\omega_s(a, \tau)$  is calculated from  $W_s$  using

$$\omega_s(a, \tau) = \frac{-i}{2\pi W_s(a, \tau)} \frac{\partial W_s(a, \tau)}{\partial \tau}, \quad \text{for } W_s(a, \tau) \neq 0. \quad (4)$$



The information from the time-scale plane is transferred to the time-frequency plane,  $(a, \tau) \rightarrow (\omega_s(a, \tau), \tau) = s(\omega, t)$ ; this operation is called synchrosqueezing (Daubechies et al., 2011). The frequency variable  $\omega$  and the scale variable  $a$  are binned; i.e.,  $W_s(a, \tau)$  is computed only at discrete values  $a_k$ , with  $a_k - a_{k-1} = (\Delta a)_k$ , and its synchrosqueezed transform  $T_s(a, \tau)$  is likewise determined only at the centers  $\omega_\ell$  of the successive bins  $[\omega_\ell - (1/2)\Delta\omega, \omega_\ell + (1/2)\Delta\omega]$ , with  $\omega_\ell - \omega_{\ell-1} = \Delta\omega$ , by summing different contributions

$$T_s(\omega_\ell, \tau) = (\Delta\omega)^{-1} \sum_{a_k : |\omega(a_k, \tau) - \omega_\ell| \leq \Delta\omega/2} W_s(a_k, \tau) a_k^{-3/2} (\Delta a)_k. \quad (5)$$

In this way, synchrosqueezing provides a concentrated representation of multicomponent signals in the time-frequency plane that allows for separating and demodulating different wave modes. The discretized version of  $T_s(\omega_\ell, \tau)$  in equation 5 can be represented by  $\tilde{T}_s(\omega_\ell, t_m)$ , where  $t_m$  is the discrete time  $t_m = t_0 + m\Delta t$ , with  $\Delta t$  is the sampling interval,  $m = 0, \dots, n - 1$ ;  $n$  is the total number of samples in the discrete signal  $\tilde{s}_m$  (Thakur et al., 2013).

Real parts of individual components  $s_k$  can be reconstructed from the real part of the discrete synchrosqueezed transform  $\tilde{T}_s$  using the inverse CWT over a narrow frequency band  $\ell \in L_k(t_m)$  around the  $k$ th component (Herrera et al., 2014)

$$s_k(t_m) = 2C_\psi^{-1} \Re e \left( \sum_{\ell \in L_k(t_m)} \tilde{T}_s(\omega_\ell, t_m) \right), \quad (6)$$

where  $C_\psi$  is a constant, which is given in Thakur et al. (2013) depending on the mother wavelet. Figure 1d shows sharpened TFR of SS-CWT compared with STFT (Figure 1b) and CWT (Figure 1c).

### Wavelet denoising

In a wavelet denoising procedure, the goal is to estimate the signal  $f(t)$  (dropping the  $k$  index) in equation 1 from observations  $s(t)$ , in a way that minimizes the mean squared error:

Figure 1. (a) Vertical component low-frequency microearthquake recorded during an underground collapse of a cavern in the Napoleonville salt dome, Louisiana. The event is located 400 m from a surface station. The sampling rate is 200 samples per second. (b) STFT, (c) CWT, and (d) SS-CWT of the time series.

$$\|f - \tilde{f}\|^2 \triangleq \frac{1}{N} \sum_{t=0}^{N-1} |f(t) - \tilde{f}(t)|^2, \quad (7)$$

where  $\tilde{f}$  is the estimated signal. Let  $W$  be the wavelet transformation. Then, the WT of the noisy signal in equation 1 can be written as

$$W_s = W_f + W_e, \quad (8)$$

where  $W_s$  is the wavelet coefficients of the observed signal,  $W_f$  is the wavelet coefficients of the seismic signal, and  $W_e$  representing the wavelet coefficients of the noise. Now, let  $\text{Thr}(\cdot)$  be a wavelet-thresholding function. Then, wavelet thresholding-based denoising schemes can be expressed as follows:

$$\tilde{f} = W^{-1}(\text{Thr}(W_s)), \quad (9)$$

where  $W^{-1}$  is the inverse WT.

The most common choices for  $\text{Thr}(\cdot)$  are “hard-” or “soft-thresholding functions.” The hard-thresholding function chooses all wavelet coefficients that are greater than a given threshold  $\lambda$  and sets the others to zero:

$$\eta_\lambda^{\text{hrd}}(W_s) = \begin{cases} W_s & \text{if } |W_s| \geq \lambda, \\ 0 & \text{otherwise,} \end{cases} \quad (10)$$

where  $\lambda \geq 0$  is the threshold level. Donoho and Johnston (1994) show that for Gaussian noise of variance  $\sigma^2$ , an optimal threshold can be  $\lambda = \sigma\sqrt{2\log_e n}$ , also known as the universal threshold, for a signal with  $n$  samples. Donoho (1995) gives  $\sigma = \text{median}(|W_s - \text{median}(W_s)|)/0.6745$  as the estimates level of noise from coefficients of the observed signal. If a wavelet coefficient is greater than  $\lambda$ , we assume that it is significant and attribute it to the original signal. Otherwise, we consider it to be due to the additive noise and discard the value.

The other popular scheme is called soft thresholding (also known as shrinkage), where wavelet coefficients are shrunk by  $\lambda$  toward zero:

$$\eta_\lambda^{\text{sft}}(W_s) = \begin{cases} W_s - \lambda & \text{if } W_s \geq \lambda, \\ 0 & \text{if } |W_s| < \lambda, \\ W_s + \lambda & \text{if } W_s \leq -\lambda. \end{cases} \quad (11)$$

Hard thresholding is known to yield abrupt artifacts in the denoised signal (Chang et al., 2000). On the other hand, it is known that soft thresholding produces smaller errors, but often results in over smoothing the denoised signal. Another option with more moderate behavior is CT proposed by Yoon and Vaidyanathan (2004), as

$$\eta_{\lambda,\gamma,\alpha}^{\text{ctm}} = \begin{cases} W_s - \text{sgn}(W_s)(1-\alpha)\lambda & \text{if, } |W_s| \geq \lambda, \\ 0 & \text{if, } |W_s| \leq \gamma, \\ \alpha\lambda \left(\frac{|W_s|-\gamma}{\lambda-\gamma}\right)^2 \left\{ (\alpha-3)\left(\frac{|W_s|-\gamma}{\lambda-\gamma}\right) + 4 - \alpha \right\} & \text{otherwise,} \end{cases} \quad (12)$$

where  $0 < \gamma < \lambda$  and  $0 \leq \alpha \leq 1$ . The  $\gamma$  is the cut-off value, below which the wavelet coefficients are set to the zero, and  $\alpha$  is a param-

eter that determines the shape of the thresholding function. This thresholding function is similar to hard thresholding but with a smooth transition around the threshold value. Hence, it can be viewed as a linear combination of hard and soft thresholding and is shown to outperform both (Yoon and Vaidyanathan, 2004).

## METHOD

The denoising method consists of the following steps: first, time series is transformed into the time-frequency domain through the CWT (equation 2). Then, after the TFT, the existence of high-power, long-duration features outside of the frequency band of microseismic events in the TFR is checked and if true, the time-frequency map is decomposed into two segments and each segment is treated differently for the denoising. Otherwise, the whole TFR is denoised similarly (using the process defined for the high-frequency segment). In this study, low-frequency features are thresholded by the soft-thresholding scheme of Donoho and Johnston (1994) (equation 11) because of its smoothing characteristics. For high-frequency features, high-energy arrival times (associated with arrivals of seismic events) will be estimated using a CF. Next, both segments are synchrosqueezed. In the SS-CWT domain, characteristics of the noise are determined from the presignal section of the high-frequency segment (based on estimated arrivals of seismic signals in previous step), and SS-CWT coefficients are normalized to attenuate dominant noise energy present in the frequency range of microseismic events. Next, the normalized coefficients of the high-frequency section and soft-thresholded coefficients of the low-frequency section are put together to form the denoised time-frequency spectrum and inverse transformed into the time domain to obtain the primary denoised signal. The denoised signal is further improved by a postdenoising step. To do so, the denoised data are transferred into CWT domain again and coefficients are thresholded using CT scheme (i.e., equation 12). Next, attenuated CWT coefficients are processed into the SS-CWT domain, and microseismic events are detected and onset times are estimated more accurately by the same CF using the cleaned spectrum.

In the following, the proposed procedure will be explained in more detail and demonstrated through application to an example of microseismic data recorded during a wastewater injection episode in central Arkansas, 2011.

### Time-frequency segmentation

Time-frequency denoising is based on the assumption that a signal's energy is concentrated in a few high-power time-frequency coefficients in a TFR, whereas noise is represented by a larger number of coefficients with small values (sparsity). In the TFR of microseismic data, where events span a short period of time and are associated with relatively lower power energy (compared with larger local or regional earthquakes), existence of other high-power features (noise or long period signals) in the time-frequency map can affect the performance of time-frequency denoising and decrease efficiency. Hence, one strategy would be to distinguish and eliminate effects of these features to increase sparsity and, as a result, increasing denoising efficiency.

To do so, after transforming the data into the time-frequency domain we separate the major features of the time-frequency map. The CWT is designed to give good time resolution and poor frequency resolution at high frequencies, and good frequency resolution and

poor time resolution at low frequencies. A common observation seen in the continuous wavelet representation of passive microseismic records is that high power features span the entire length of data within some limited frequency bands. Some of these features relate to dominant noise in relatively narrow frequency bands within the frequency range of the microearthquake events. Others occur in relatively lower-frequency bands (higher scales) outside of the dominant-frequency range of microseismic events. On the other hand, high-frequency (low scale) and time-localizing features (low scales) that correspond to the seismic events do not last for the entire duration of the time series and appear from time to time as short bursts (Figure 2c). We use this characteristic to separate high-power low-frequency features out of the frequency range of microseismic events. To do this, a CF of the stacked amplitude of CWT coefficients is calculated using all scales:

$$\text{CF}(\tau) = \sum_{\tau=1}^n |W_s(a, \tau)| \quad \text{for } a = 1, \dots, n_a, \quad (13)$$

where  $n_a$  is the number of scales. The CF gives the distribution of coefficient magnitudes along the scale axis. The existence of low-frequency features causes this function to have two distinct peaks (Figure 2b). We check this by distinguishing between unimodality and bimodality of a smoothed version of this function using Akaike's (1974) information criterion difference (AICdiff; Appendix A).

Once high-power low-frequency features are found from the bimodality of the CF, the low- and high-frequency components of the waveform are separated by finding an optimum threshold scale factor  $a^*$  using Otsu's (1979) method (Appendix B). This optimal value can separate wavelet coefficients into two clusters (Figure 2b).

Using  $a^*$ , wavelet coefficients are divided into two segments with the upper segment containing coefficients associated with lower frequency components (Figure 2d) and the lower segment with coefficients of the higher frequency components (Figure 2e).

## Thresholding

Low-frequency features can be removed by high-frequency filtering for event detection and onset-time estimation purposes. The segmentation procedure proposed in the previous section can be interpreted as an automatic process for checking the existence of low-frequency, long-duration features and finding the optimal corner frequency for high-pass filtering. However, for more general denoising purposes, the low-frequency segment can be thresholded to preserve nonnoise features in this frequency band. For example, non-noise features can be long-period, long-duration signals observed in some hydraulic fracturing experiments (Zoback et al., 2012; Eaton et al., 2013) or very long-period (VLP) signals observed in some mining induced cases (Mousavi et al., 2015). Due to the smooth characteristics of low-frequency features, this segment is thresholded separately using the soft-thresholding scheme of equation 11 (Figure 3a and 3c).

Dominant noise within the microseismic-frequency band is distinguished and attenuated within the high-frequency segment. To do so, data are transferred into the SS-CWT domain (Figure 3b). Dominant frequency bands of the noise within the signal's frequency range are determined from the high-resolution structure of noise coefficients in a time window from the beginning of the time series to the first high-energy arrival. High-energy arrival times (Figure 2f) are estimated using a CF, a DF, which will be explained in the next section.

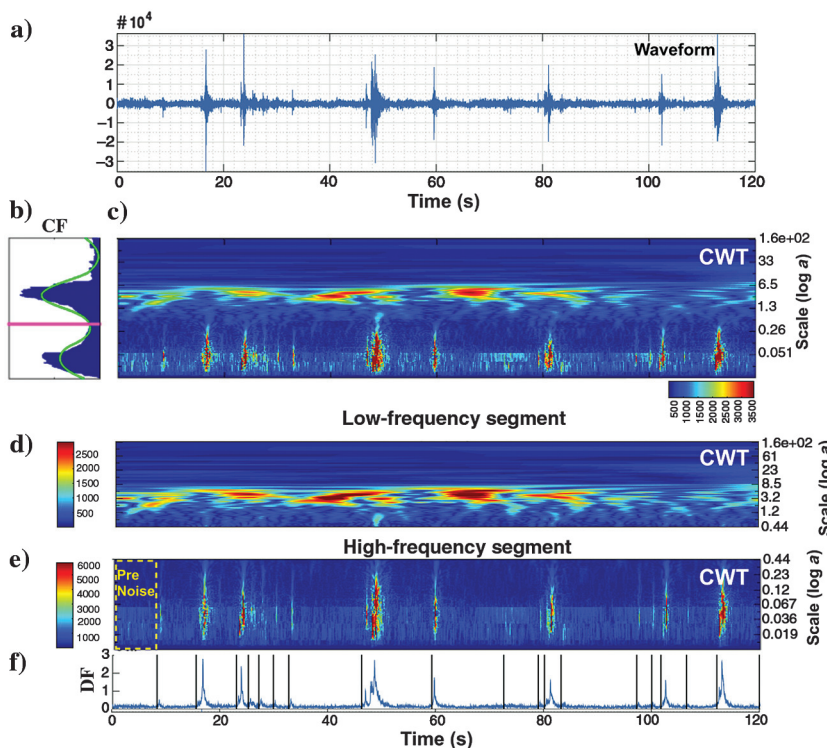


Figure 2. (a) Two-minute vertical component recording of microseismic events induced by waste water injection in central Arkansas. Events are recorded by a broadband sensor, station CH2 at 35.3341N, -92.2982W, at the surface in 2011. Hypocentral distances range between 1.7 and 2.5 km and event size ranges between  $-0.5$  and  $0.38 M_w$ . (b) Histogram of the stacked function CF. The smoothed function used for the Gaussian fit is shown by the green line. The optimal scale value for separating long-period and high-frequency coefficients selected by Otsu's method is shown with the horizontal magenta line. (c) The continuous wavelet scalogram of data. (d) The scalogram of the low-frequency segment. (e) The scalogram of the high-frequency segment and presignal noise section. (f) The function DF (equation 15) showing the cumulative energy distribution. Black lines define the arrival of high-energy signals.

Using the presignal noise, dominant coefficients are first highlighted by hard thresholding (equation 10) to keep the stronger noise coefficients. Then, the CF (equation 13) is used to determine frequency bands with highest noise energy (Figure 3e). In this way, the coefficients representing the dominant components of the noise are detected and then normalized in each frequency band by

$$\begin{cases} T_r = T_r \times \frac{(|T_r| - M_{\max})}{|T_r|} & \text{If } |T_r| > M_{\max}, \\ T_r = 0 & \text{If } \lambda_n < |T_r| \leq M_{\max}, \\ T_r = \frac{T_r}{\lambda_n} & \text{If } \lambda_n > |T_r|, \end{cases} \quad (14)$$

where  $M_{\max} = \text{mean}(\max |T_n|)$ ,  $T_r$  and  $T_n$  are the SS-CWT coefficients within each narrow frequency band, respectively. With this normalization step, we basically attenuate the high-power coefficients associated with noise and increase the sparsity of the TFR (Figure 3d and 3f).

In the next step, the normalized coefficients for the high-frequency section and thresholded coefficients of the low-frequency section are put together and inverse SS-CWT transformed to obtain the initial estimation of the signal  $f$ . This initial estimation will be improved by a postprocessing step to obtain the final denoised signal. This is done by transforming again into the CWT domain and applying the CT of equation 12. For CT, the optimal threshold values are chosen at each scale based on the wavelet coefficients of presignal noise, and the coefficients are thresholded scale by scale. Thresholded coefficients are then processed in the SS-CWT domain to detect events and to estimate onset times using the procedure explained in the next section. The final denoised signal is obtained by inverse transforming the denoised coefficients into the time domain (Figure 4).

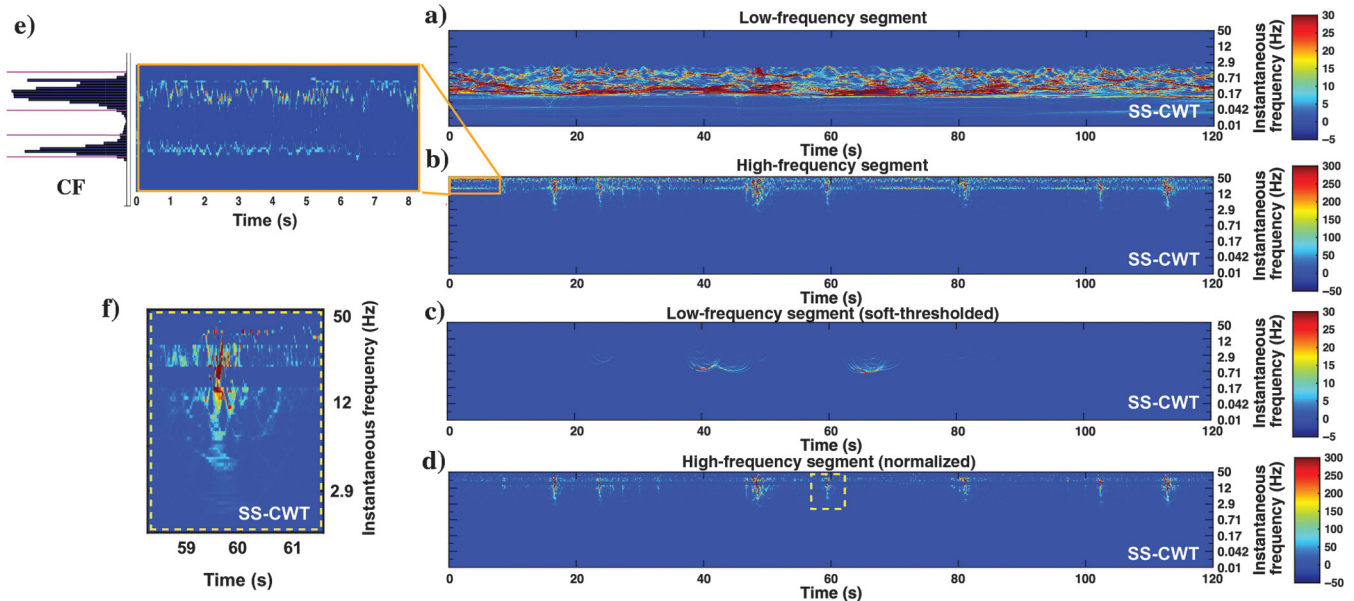


Figure 3. (a) The SS-CWT spectrogram of low-frequency segment. (b) The SS-CWT of high-frequency segment. It is obvious from the spectrogram that most of the noise energy is concentrated in two narrow frequency bands. (c) The SS-CWT spectrogram of low-frequency segment after soft thresholding. (d) The SS-CWT spectrogram of high-frequency segment after normalization. (e) The magnified window of presignal noise section (shown in Figure 2e with the box) and the stacked CF and picked narrow bands around its major peaks. Horizontal lines show frequency bands where the dominant energy of noise exists. (f) Magnified window around SS-CWT spectrogram of an event in the after normalization.

## Arrival time detection

The most precise time localization of wave arrivals based on the CWT coefficients is obtained at smaller scales. This characteristic of the CWT is very useful for detecting abrupt changes in a continuous record associated with seismic signal arrivals. Abrupt changes in a seismic record produce relatively large wavelet coefficients (in absolute value) centered around the discontinuity. The following CFs are defined to capture these abrupt changes in energy distribution in the TFR and to estimate arrival times of microseismic events.

First, the function DF is calculated by stacking of multiscale envelopes of the time-frequency coefficients (Figure 5b):

$$\text{DF}(a) = \sum_{a=1}^{n_a} |E(a, \tau)| \quad \text{for } \tau = 1, \dots, n, \quad (15)$$

where  $n_a$  is the number of scales and  $E(a, \tau)$  is the envelope function of CWT coefficients for scale  $a$  (Kanasewich, 1981) and defined as

$$E(a) = \sum_{\tau=1}^n \sqrt{W_s(a, \tau)^2 + \bar{W}_s(a, \tau)^2}, \quad (16)$$

where  $\bar{W}_s$  is the Hilbert transform of the time-frequency coefficients. Then, the running energy ratio is calculated using DF:

$$\text{ER}_1(\tau) = \frac{\sum_{i=\tau}^{\tau+L} \text{DF}(i)}{\sum_{i=\tau-L}^{\tau} \text{DF}(i)}, \quad (17)$$

where  $L$  is the length of the energy collection window preceding and following the test point at  $\tau$ . The final arrival-time

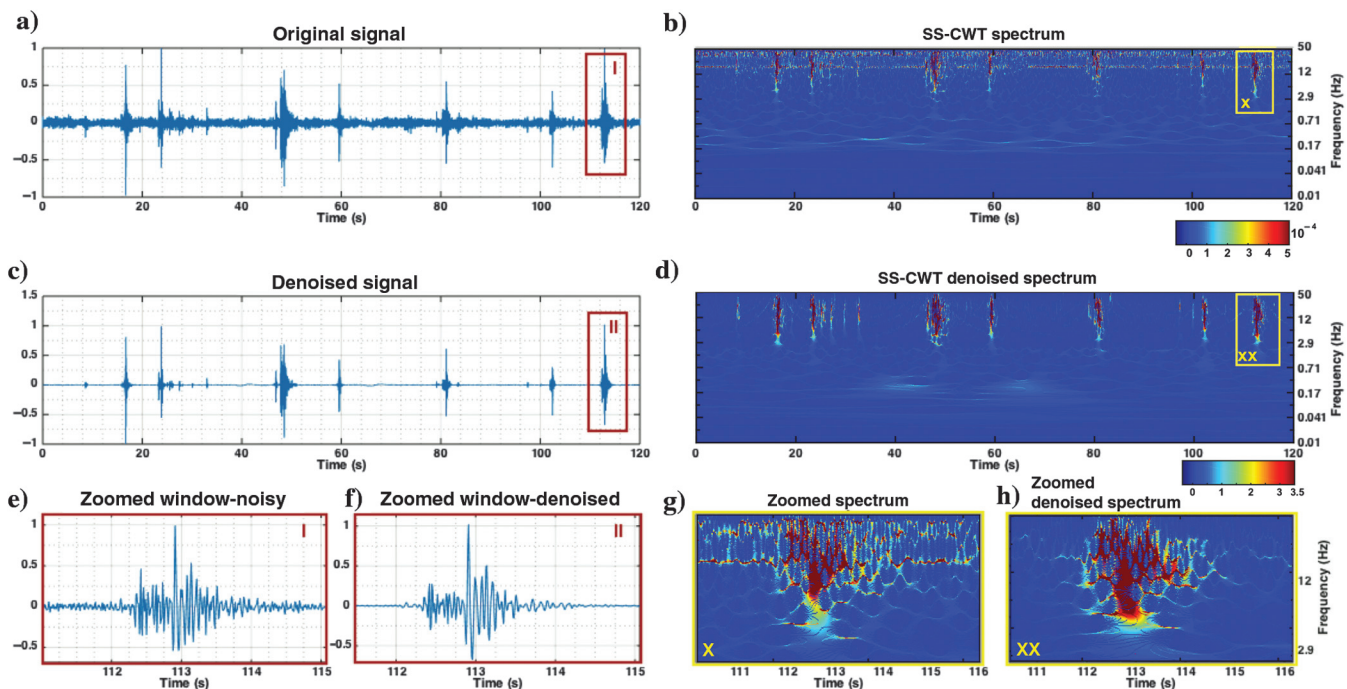


Figure 4. (a) Original seismogram of several microseismic events induced by waste fluid injection in central Arkansas. (b) The SS-CWT spectrum of the original data, (c) denoised seismogram and (d) associated spectrogram, respectively, (e) magnified windows of the original and (f) denoised signal around one event, respectively. (g and h) The SS-CWT representations of the same event as panels (e and f). The X and XX indicate the magnified boxes (g and h), respectively.

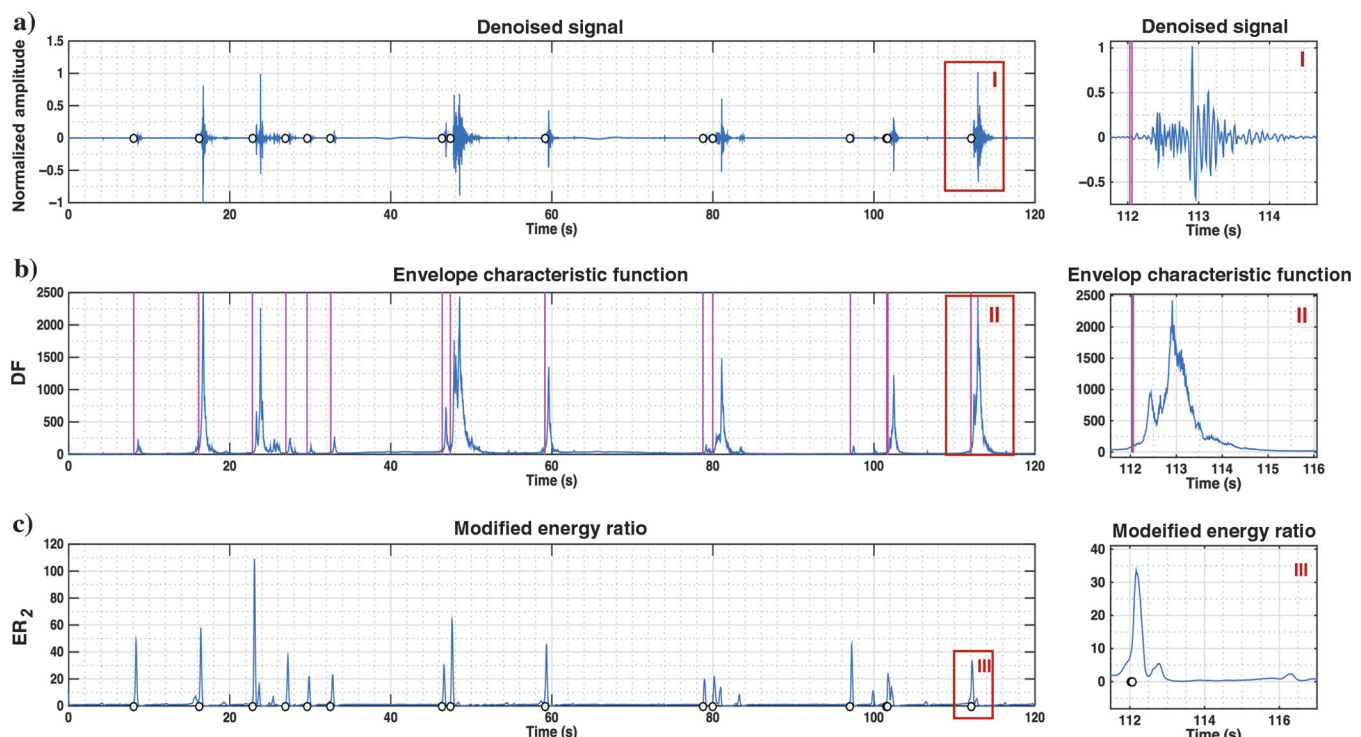


Figure 5. (a) The denoised signal and detected events indicated by open circles. In addition, a magnified window gives a closer view of one detected event. (b) The envelope characteristic function DF, and onset detections (vertical lines). (c) Modified energy ratio ER<sub>2</sub>. Circles are indication of detected events where local maxima of ER<sub>2</sub> pass the threshold value. Vertical lines indicate onset times of seismic events and are associated with the time when value of DF start to rise (positive slope) and coincide with the local maxima of ER<sub>2</sub>.

estimate of the high-energy seismic signal is obtained by computing

$$\text{ER}_2(\tau) = \text{ER}_1(\tau)|\text{DF}(a)| \quad (18)$$

and finding the local maxima of  $\text{ER}_2$ , which pass a given threshold value (Figure 5c). The threshold value is set to be a fraction of the maximum peak value and defines the sensitivity of detection.

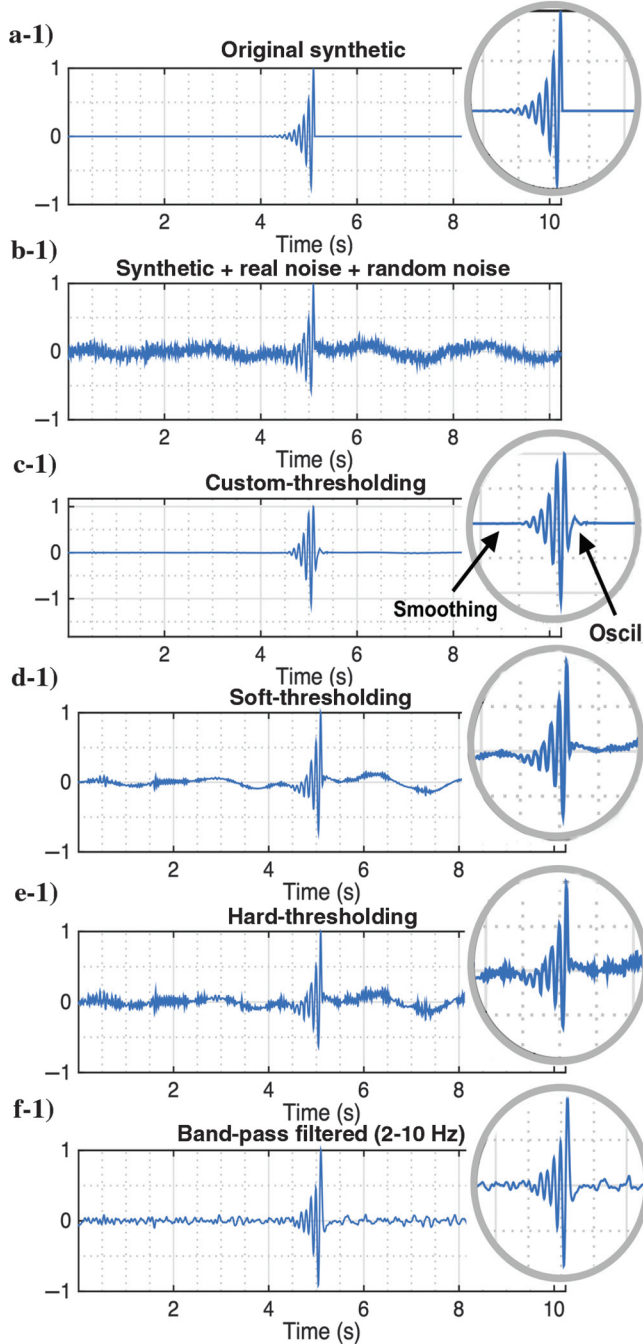
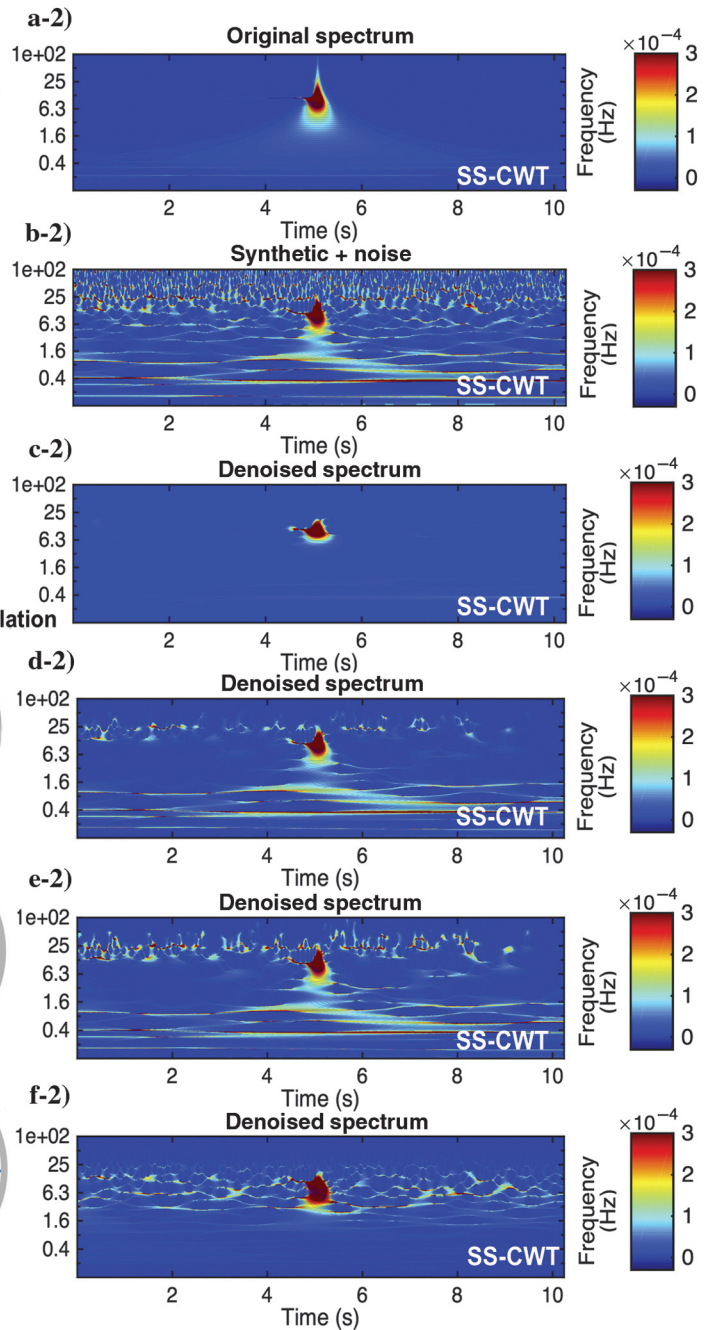


Figure 6. (a) The synthetic signal (a-1) and its SS-CWT (a-2). (b) The synthetic signal contaminated with field seismic noise and its transform. (c) The denoised signal using the proposed method and its transform. (d) The denoised signal using the standard soft-thresholding method and its transform, and (e) the denoised signal using the standard hard-thresholding method and its transform. (f) Band-pass filtered data between 2 and 10 Hz.

## RESULTS

### Synthetic tests

The denoising algorithm is applied to a known synthetic signal, which is contaminated with the field seismic noise. We generated a simple pulse signal (similar to Galiana-Marino, 2008) as the synthetic with a dominant frequency of 7 Hz using a sampling frequency of 200 Hz and damping factor of -6 (Figure 6a). This



signal was designed to model low-frequency microearthquakes recorded at the surface. Moreover, our goal was to observe the effects of the denoising process on the polarity, time shift, and smoothing of very small emergent arrivals at the very beginning of the signal buried under the background noise and track the changes on other parts more easily. This signal was then contaminated with field seismic noise recorded by a surface broadband station during microseismic monitoring at Bayou Corne, Louisiana, and additional random noise for a resulting S/N of three (Figure 6b). In our implementation of the SS-CWT, we use a Morlet wavelet as the mother wavelet with 64 voices per octave. This was based on the crosscorrelation results of a small window around the maximum amplitude of the synthetic pulse and several different wavelets. Moreover, in testing different wavelets, we observed that the Morlet, Shannon, and Hshannon wavelets tends to emphasize the noise structure as well as discontinuities in a signal, such as the one associated with the first seismic arrival. Other wavelets, such as the Mexican hat wavelet, had the opposite effect. Selection of wavelet type based on the seismic signal can be automated and be more adaptive to the signal nature using methods suggested by [Bogiatzis and Ishii \(2015\)](#).

The result of our denoising approach was compared with frequency filtering and traditional thresholding methods using other TFR.

Custom thresholding was done automatically for 54 different combinations of  $\gamma$  (equation 12) (varying between 0.1 and 0.9 with a 0.1 increment) and  $\alpha$  (varying between 0 and 1 with a 0.2 increment), and the denoised result with the minimum root-mean-squared (rms) difference to the original signal was selected as the denoised signal.

The original signal, the noise-contaminated one, and the denoised signals using the proposed method, soft-thresholding, hard-thresholding, and band-pass filtering are presented along with their SS-CWT representations in Figure 6. Figure 6b-2 shows that the entire time-frequency plane exhibits signals of different amplitudes but with more dispersed frequency components and continuity in time indicating the presence of noise.

As can be seen from Figure 6, the best result in terms of removing most of the noise within different frequency bands was obtained by our proposed method (Figure 6c-1 and 6c-2). The highest crosscorrelation (0.945), S/N (178.8), and lowest rms error (0.035) were obtained (Table 1). However, this method was very computationally expensive (39.97 s). Comparing performance of soft and hard thresholding, soft thresholding achieved relatively better results. In soft and hard thresholding, some high- and low-frequency noises were left (Figure 6d-2 and 6e-2). On the other hand, band-pass filtering left the noises with the same frequency band as the signal untouched (Figure 6f-2). The most similar spectral structure to the original structure of the signal was obtained by the custom procedure proposed in this study by removing most of the noise (compare Figure 6a-2 and 6c-2). The common features between denoised signals are small oscillations at the end of the signal and smoothing of the emergent arrival (Figure 6c-1–6f-1). [Galiana-Marino et al. \(2008\)](#) also observe these kinds of oscillations in wavelet-based denoising methods and suggest that it can be reduced by better selection of the maximum decomposition level. If we compare the results based on preserving small-amplitude emergent arrivals approximately 4.5 s, spectral filtering (Figure 6f-1) was not successful in revealing these small features. Many small amplitude and similar features associated with the noise remained in the waveform. Our

customized denoising process did a better job in preserving small amplitude features of the signal after 4.5 s.

Compared with soft and hard thresholding, CT changed the amplitude of the signal, which is expected due to the normalization step on the SS-CWT coefficients, but the polarization remains unchanged and the overall shape of the signal is better retained. The emergent arrival of the reconstructed signal is clearer than on the noise-contaminated one (Figure 6b-1), indicating that phase picking would be better performed using the denoised signal.

## Field seismic data

We applied the method to passively recorded, high-noise microseismic data to test the efficiency of the method in denoising, automatic detection, and first-arrival time estimation. Data were recorded by a broadband seismometer located at the surface in Bayou Corne, Louisiana, during microseismic monitoring of the area in 2013. Microseismic events were associated with the underground collapse of a cavern within the Napoleonville salt dome. Events are located within the caprock and salt body, 400–1200 m from the receiver and their moment magnitudes range from  $M_w$  –1.7 to 0.59. The rms amplitude of the signal of the selected event in Figure 7 to the preceding noise (S/N) is 1.1, which is insufficient to determine a precise arrival time. Band-pass filtering within the band of 1–10 Hz increases the S/N to 4.13. We applied our denoising method to 2.5 h of vertical component data. The proposed method removed most of the noise and increased the S/N of the selected event to 12.63 (Figure 7b).

Testing the proposed method and a standard STA/LTA algorithm on the data gives close results in terms of the detection rate; the denoising-based method of this study yielded a detection of 16 events out of 18 events presented in the time series and, STA/LTA detected 14 events. However, it seems that the denoising-based method is more sensitive to the detection of small and close events in time (compare the two extra events detected by this method presented in magnified windows in Figure 7 and two sample events detected by STA/LTA in Figure 8). Moreover, in the proposed method, the CF triggers very close to the time of first arrivals, whereas STA/LTA does not yield an accurate onset detection.

We compare the detected onsets for some events obtained with the two methods (Figure 9). This clearly illustrates the good performance of the proposed method by improving the S/N and accuracy of the onset detection. We can see clearly that thresholding times for the denoised-based method appear to be very close to the onset time, whereas STA/LTA does not have this capability.

**Table 1. The rms error (rms) S/N, maximum crosscorrelation coefficients between denoised and original signal (before adding the noise) (CC), and computational time of the synthetic test for different thresholding methods.**

	rms	S/N	CC	Time lapse (s)
Custom thresholding	0.0352	178.8	0.945	39.974
Soft thresholding	0.0605	6.2	0.767	0.972
Hard thresholding	0.0661	4.8	0.721	0.918
Band-pass filtering	0.0411	9.8	0.889	0.159

In Figure 9a, STA/LTA was triggered with two cycles' delay compared with the onset time, whereas the proposed method was very sensitive to a very emergent pulse before the first impulsive arrival. Although denoised and filtered waveforms look slightly different, but from band-pass filtered data (on right), it can be seen that the picked onset time (on left) occurred at the same time as the upward impulsive arrival. More or less, the same pattern (earlier picks by the proposed method compared with STA/LTA) is observed in Figure 9b, 9d, 9e, 9f, and 9h, in which picked onset times using both methods are close (within one to three cycles and less than 1 s), but with more accurate onset times for emergent arrivals for the proposed method of this study. However, in Figure 9c, there is more than 3.5 s time delay for the arrival time picked by STA/LTA, whereas the onset time picked by the time-frequency method of this

study is very close to the actual first arrival time. This implies more consistent results for the proposed method. Although, in Figure 9g, the onset time picked by the proposed method looks relatively early. However, this is less than 0.5 s and coincides with a very emergent pulse prior to the impulsive arrival.

## DISCUSSION

The main advantage of the SS-CWT transform is its high resolution and decomposition properties that makes the identification of the spectral structure of the noise possible and improves the efficiency of thresholding by increasing the sparsity of the TFR through a normalization step.

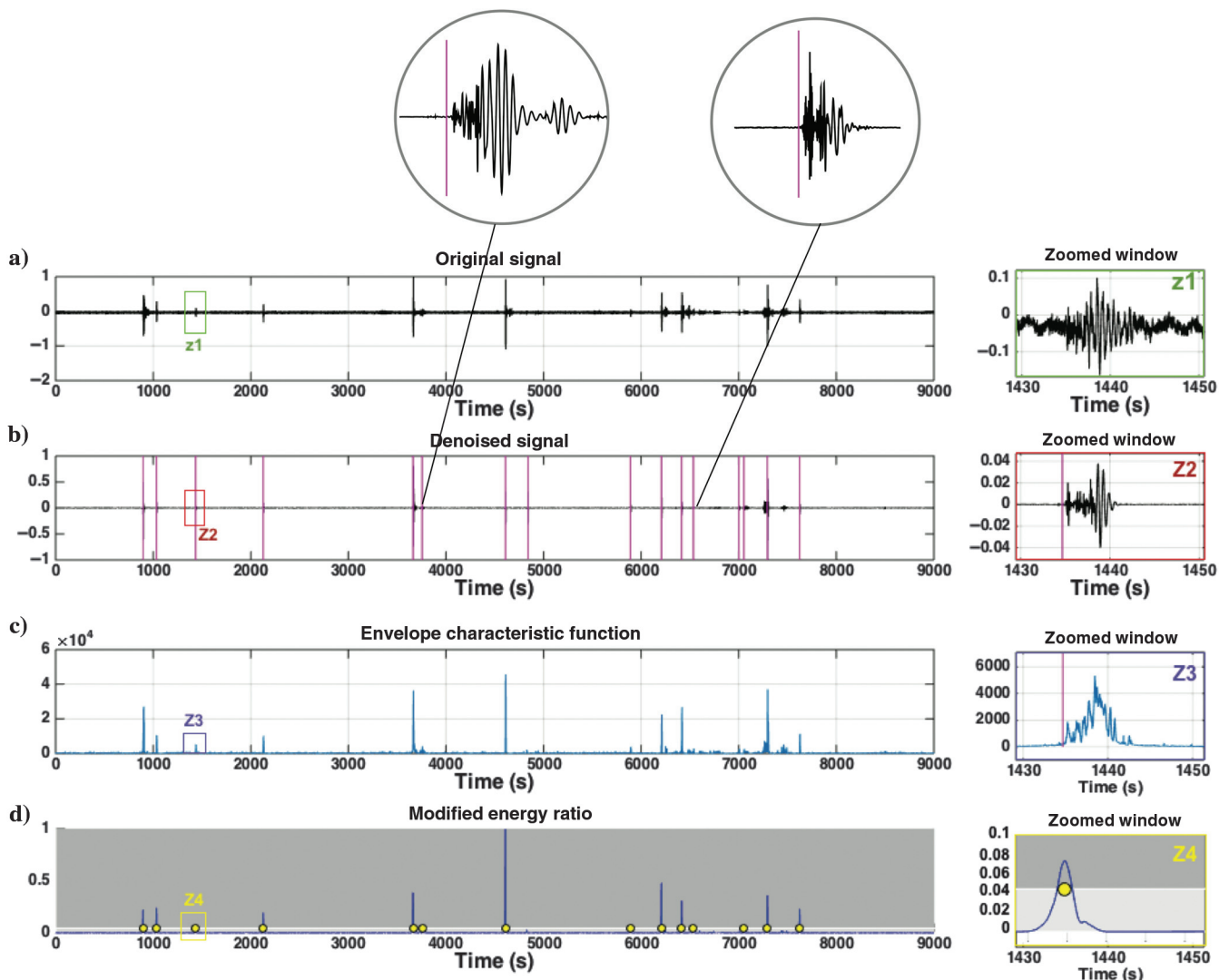


Figure 7. Field microseismic data after the denoising and detection using the proposed method. (a) Vertical ground motion showing microseismic events recorded at station LA14 at Bayou Corne, Louisiana, in October 2013 and a magnified window (Z1) around a selected event. (b) The denoised seismogram using the proposed method and a magnified window (Z2) showing a closer view of the event after denoising onset pick. Vertical lines indicate onset-time estimations associated with local maxima and triggering points on the energy ratio function. Two magnified windows on top show extra events detected by this method compared with the STA/LTA. (c) The characteristic function DF, calculated from the energy envelope. (d) The blue solid line is the ER<sub>2</sub> function, the light gray area shows the threshold limit (15% of max) for the detection triggering, and the circles indicate local maxima in the ER<sub>2</sub> that pass the threshold limit. The magnified window (Z4) shows the function associated to one detected event.

Simultaneous denoising and detection is shown to increase the accuracy of onset detection improving the efficiency of event detection. Because of the inherent crosscorrelation characteristic of the CWT, the proposed method can be compared with the denoising method of Eisner et al. (2008). In match filtering (also known as the master-slave method) one event with high S/N is selected as the master event, a very narrow window around the peak amplitude is zero-lag crosscorrelated with the continuous waveform, and then the crosscorrelation coefficient traces from different stations are stacked to increase the S/N. The success of this method is based on the inherent ability of the crosscorrelation to match similar events and automatically remove the moveouts between the resulting coefficient traces. However, the selection of one master event is the factor in the process that limits the efficiency of the method to similar events with close hypocenters and similar mechanisms. In

the CWT-based method discussed in this paper, a mother wavelet with high correlation with the maximum energy of one event (equivalent to the master event) is selected, and it is used in the crosscorrelation with the continuous record. The flexibility of the method is increased by the scaling procedure of the mother wavelet. The CF (equation 18) can be interpreted as stacking the envelopes of hundreds of traces of crosscorrelation values, where each trace is the result of the crosscorrelation with a different scaled mother wavelet. This flexibility can be further improved by a more complicated automatic selection of the appropriate mother wavelet based on the nature of the data set or using part of a master event's signal as the mother wavelet. This can simulate the use of secondary master events, or cousin events, in crosscorrelation-based detection methods. Opposite to the efficiency-based objective of match filtering, the objective of the proposed method is to clear up the signal

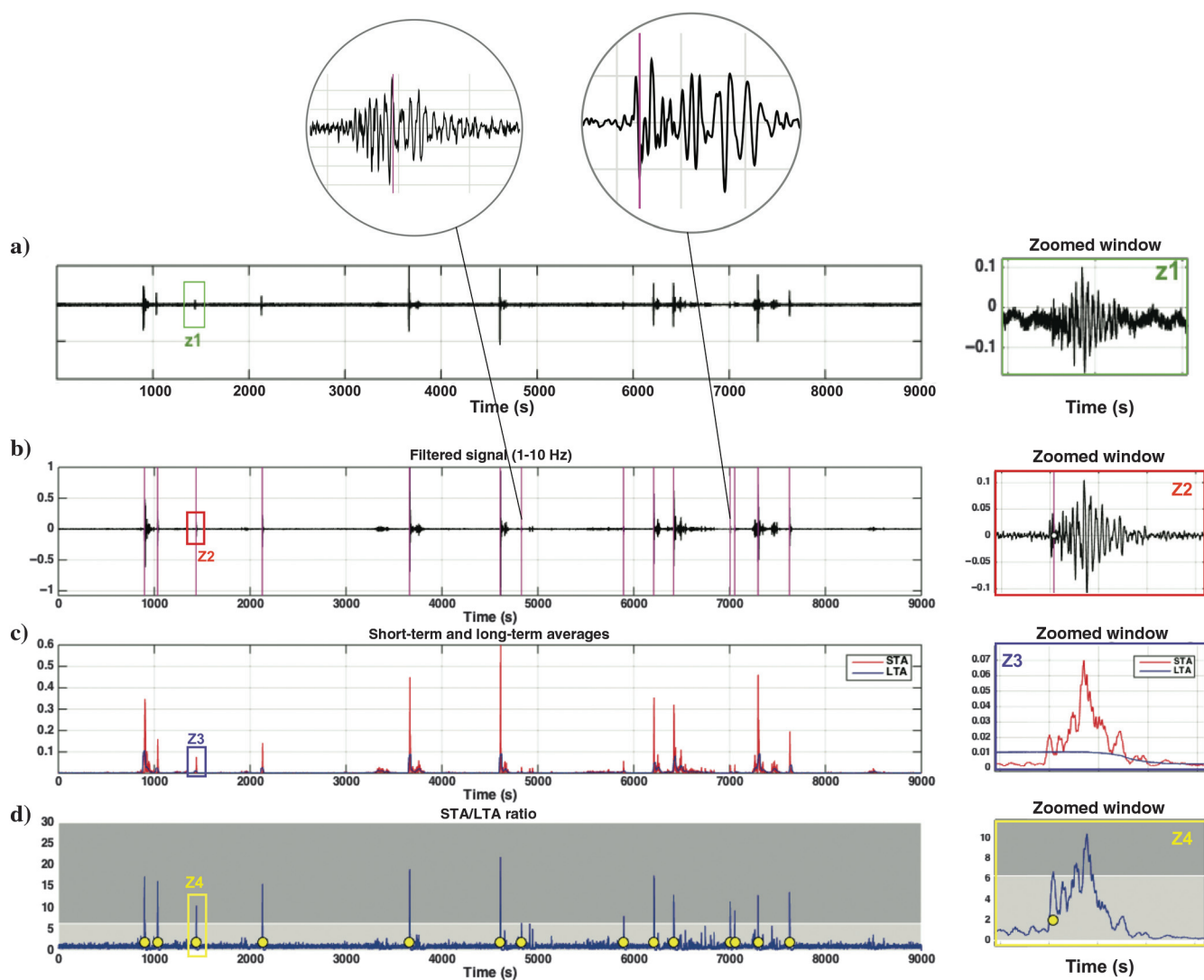


Figure 8. Field microseismic data after band-pass filtering and detection using the STA/LTA method. (a) Vertical ground-motion record of microseismic events. Same scheme as in Figure 7. (b) The data have been band-pass filtered between 1 and 10 Hz, and a magnified window associated with the same event as in Figure 7 is shown (Z2). Vertical lines indicate triggering points on STA/LTA function. Two magnified windows on top show two examples of detected events. A delay between the onset time and triggering point can be seen from these small windows. (c) The STA and LTA functions. (d) The STA/LTA function. The light-gray area represents the threshold limit, and circles indicate where the STA/LTA ratio passes the threshold limit.

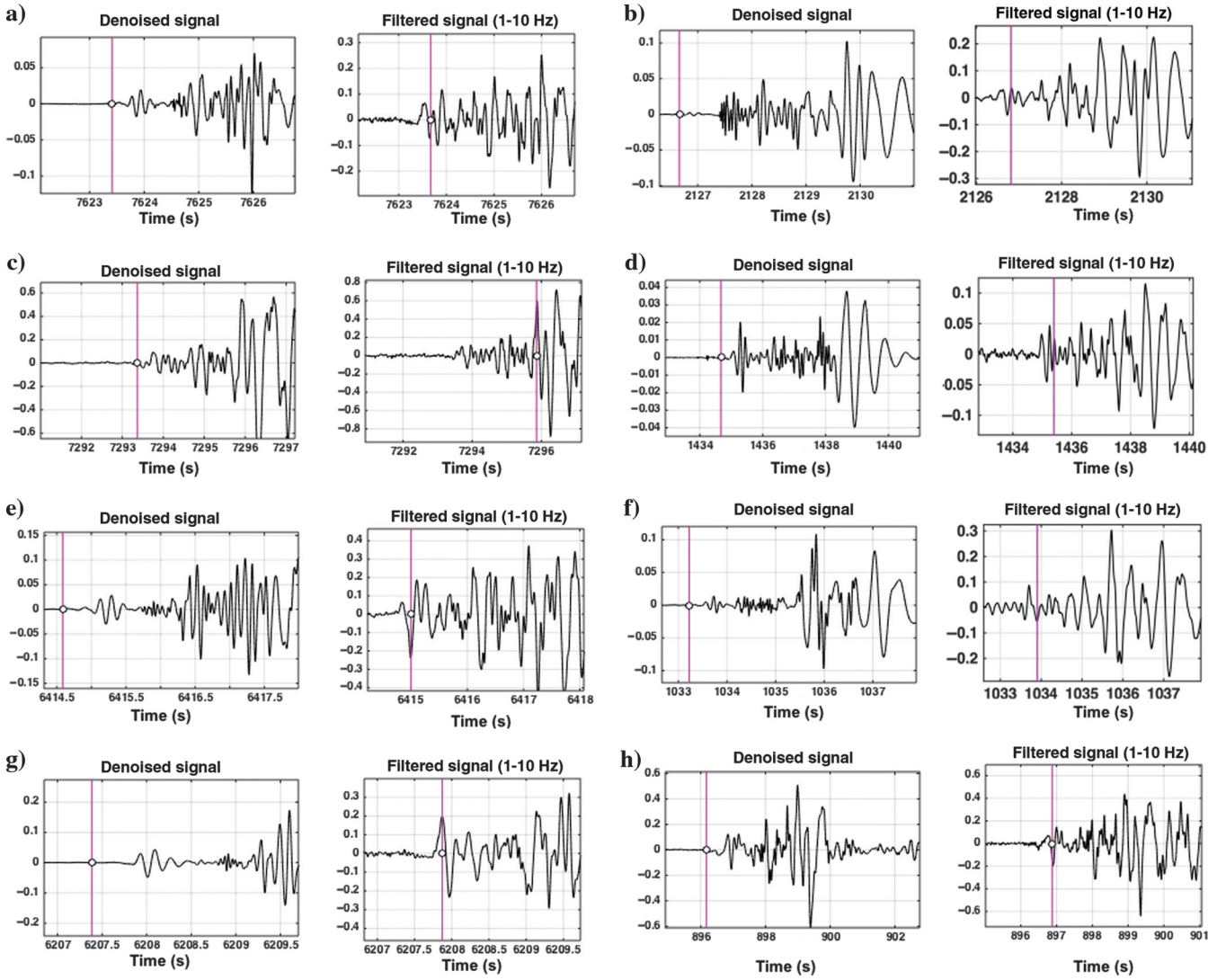


Figure 9. Magnified windows around the beginning of eight events are detected by both methods. In each panel, the left column shows denoised seismograms and triggering points (vertical lines and circles) associated to the maxima of defined CF ( $ER_2$ ), and right columns are band-pass filtered seismograms and triggering points (vertical lines) based on STA/LTA function. A delay between onset time and triggering points is observed on events detected by STA/LTA, while triggering points on the denoised seismograms occurred right before very emergent arrivals at the beginning of the signals.

and provide clearer phase arrivals with minimum distortion and loss of information rather than just increasing the S/N. The only drawback to this approach is that it is computationally more expensive.

The suggested approach brings together the advantages of time-frequency methods, crosscorrelation methods, and windowed energy ratio methods to increase the efficiency and the reliability of microseismic processing. However, the proposed method can have other applications, such as attenuation estimations. Denoising the signal can assemble the spectral content more precisely and decrease the uncertainties in  $Q$  estimation (McNamara et al., 2012; Mousavi et al., 2014), improving the ability of models to match observations.

## CONCLUSION

In this study, we have proposed a new denoising and automatic onset detection algorithm based on the SSCWT and CT. We have

compared the proposed method with conventional denoising methods of soft and hard thresholding and the well-known STA/LTA method for event detection. The proposed method has been applied to synthetic and field seismic data. The denoising method presented in this paper dynamically adapts to the characteristics of the signal. Results show that the new method considerably improves S/N and onset detection compared with conventional methods.

## ACKNOWLEDGMENTS

We would like to thank M. Withers for his comments on a pre-print of the manuscript. This study was supported by the Air Force Research Laboratory under contract number FA9453-16-C-0015 and partially by a contract from the Louisiana Department of Natural Resources. Arkansas and Bayou Corne seismic data used in this study are archived at IRIS/DMC. We thank the editor,

assistant editor, and associate editor of the *GEOPHYSICS*, and four anonymous reviewers for their careful reviews and insightful remarks.

## APPENDIX A

### CHECKING THE MODALITY OF THE CHARACTERISTIC FUNCTION

The AIC is a goodness-of-fit measure for an estimated statistical model, with lower AIC values indicating a better fit. To assess the modality of a distribution, one can fit the observed data using a 1C (i.e., unimodal) and 2C (i.e., bimodal) Gaussian distribution model to determine which of the two models minimizes the AIC (McLachlan and Peel, 2000). If the 1C model minimizes the AIC, the distribution is better described as unimodal, and if the 2C model minimizes the AIC, the distribution is better described as a bimodal. A proportional difference score (AICdiff) for the two models (1C, AIC1; 2C, AIC2) can be calculated as (Wagenmakers and Farrell, 2004)

$$\text{AICdiff} = \frac{\text{AIC1}-\text{AIC2}}{\max(\text{AIC1}, \text{AIC2})}, \quad (\text{A-1})$$

where AICdiff values range from  $-1$  to  $1$ , with positive values suggesting the bimodality and negative values suggesting unimodality.

## APPENDIX B

### FINDING OPTIMAL SCALE USING OTSU'S METHOD

A histogram is constructed using the elements of CF and is normalized with regard to the following probability distribution after Otsu (1979):

$$\begin{aligned} O_\omega(a) &= \sum_{i=1}^a \left( \frac{\text{CF}}{\max(\text{CF})} \right)_i, \\ O_\mu(a) &= \sum_{i=1}^a i \left( \frac{\text{CF}}{\max(\text{CF})} \right)_i, \quad \text{and} \\ O_{\mu T} &= O_\mu(n_a). \end{aligned} \quad (\text{B-1})$$

The threshold that minimizes the weighted within-class variance is calculated by

$$\sigma_B^2(a) = \frac{[O_{\mu T} O_\omega(a) - O_\mu(a)]^2}{O_\omega(a)[1 - O_\omega(a)]}, \quad (\text{B-2})$$

and the optimal threshold  $a^*$  is

$$\sigma_B^2(a^*) = \max_{1 \leq a < n_a} \sigma_B^2(a). \quad (\text{B-3})$$

## REFERENCES

- Aguiar, A. C., and G. C. Beroza, 2014, PageRank for earthquakes: *Seismological Research Letters*, **85**, 344–350, doi: [10.1785/0220130162](https://doi.org/10.1785/0220130162).
- Akaike, H., 1974, A new look at the statistical model identification: *IEEE Transactions on Automatic Control*, **19**, 716–723, doi: [10.1109/TAC.1974.1100705](https://doi.org/10.1109/TAC.1974.1100705).
- Allen, R. V., 1978, Automatic earthquake recognition and timing from signal traces: *Bulletin of Seismological Society of America*, **68**, 1521–1532.
- Amoroso, O., N. Maercklin, and A. Zollo, 2012, S-wave identification by polarization filtering and waveform coherence analyses: *Bulletin of Seismological Society of America*, **102**, 854–861, doi: [10.1785/0120110140](https://doi.org/10.1785/0120110140).
- Anant, K. S., and F. U. Dowla, 1997, Wavelet transform methods for phase identification in three-component seismograms: *Bulletin of Seismological Society of America*, **87**, 1598–1612.
- Anderson, S., and A. Nehorai, 1996, Analysis of a polarized seismic wave model: *IEEE Transaction on Signal Processing*, **44**, 379–386, doi: [10.1109/78.485933](https://doi.org/10.1109/78.485933).
- Auger, F., P. Flandrin, Y. T. Lin, S. McLaughlin, S. Meignen, T. Oberlin, and H. T. Wu, 2013, Time-frequency reassignment and synchrosqueezing: An overview: *IEEE Signal Processing Magazine*, **30**, 32–41, doi: [10.1109/MSP.2013.2265136](https://doi.org/10.1109/MSP.2013.2265136).
- Baillard, C., W. C. Crawford, V. Ballu, C. Hibert, and A. Mangeney, 2014, An automatic kurtosis-based P- and S-phase picker designed for local seismic networks: *Bulletin of Seismological Society of America*, **104**, 394–409, doi: [10.1785/0120120347](https://doi.org/10.1785/0120120347).
- Barrett, S. A., and G. C. Beroza, 2014, An empirical approach to subspace detection: *Seismological Research Letters*, **85**, 594–600, doi: [10.1785/0220130152](https://doi.org/10.1785/0220130152).
- Bekara, M., and M. van der Baan, 2009, Random and coherent noise attenuation by empirical mode decomposition: *Geophysics*, **74**, no. 5, V89–V98, doi: [10.1190/1.3157244](https://doi.org/10.1190/1.3157244).
- Berard, M., and U. Kradolfer, 1997, An automatic phase picker for local and teleseismic events: *Bulletin of Seismological Society of America*, **77**, 1437–1445.
- Bogiatzis, P., and M. Ishii, 2015, Continuous wavelet decomposition algorithms for automatic detection of compressional- and shear-wave arrival times: *Bulletin of Seismological Society of America*, **105**, 1628–1641, doi: [10.1785/0120140267](https://doi.org/10.1785/0120140267).
- Botella, F., J. Rosa-Herranz, J. J. Giner, S. Molina, and J. J. Galiana-Merino, 2003, A real-time earthquake detector with prefiltering by wavelets: *Computers and Geoscience*, **29**, 911–919, doi: [10.1016/S0098-3004\(03\)00099-2](https://doi.org/10.1016/S0098-3004(03)00099-2).
- Chang, S. G., B. Yu, and M. Vetterli, 2000, Adaptive wavelet thresholding for image denoising and compression: *IEEE Transaction on Image Processing*, **9**, 1532–1546, doi: [10.1109/83.862633](https://doi.org/10.1109/83.862633).
- Chen, Y., and J. Ma, 2014, Random noise attenuation by f-x empirical mode decomposition predictive filtering: *Geophysics*, **79**, no. 3, V81–V91, doi: [10.1190/geo2013-0080.1](https://doi.org/10.1190/geo2013-0080.1).
- Christoffersson, A., E. S. Husebye, and S. F. Ingate, 1988, Wavelet decomposition using ML-probabilities in modeling single-site 3-component records: *Geophysical Journal International*, **93**, 197–213, doi: [10.1111/j.1365-246X.1988.tb01996.x](https://doi.org/10.1111/j.1365-246X.1988.tb01996.x).
- Chu, C. K., and J. Mendel, 1994, First break refraction event picking using fuzzy logic systems: *IEEE Transaction on Fuzzy Systems*, **2**, 255–266, doi: [10.1109/91.324805](https://doi.org/10.1109/91.324805).
- Dai, H., and C. MacBeth, 1995, Automatic picking of seismic arrivals in local earthquake data using an artificial neural network: *Geophysical Journal International*, **120**, 758–774, doi: [10.1111/j.1365-246X.1995.tb01851.x](https://doi.org/10.1111/j.1365-246X.1995.tb01851.x).
- Dai, H., and C. MacBeth, 1997, The application of back-propagation neural network to automatic picking seismic arrivals from single-component recordings: *Journal of Geophysical Research*, **102**, 15105–15113, doi: [10.1029/97JB00625](https://doi.org/10.1029/97JB00625).
- Das, I., and M. D. Zoback, 2011, Long period long duration seismic events during hydraulic fracture stimulation of a shale gas reservoir: The Leading Edge, **30**, 778–786, doi: [10.1190/1.3609093](https://doi.org/10.1190/1.3609093).
- Daubechies, I., 1988, Orthonormal bases of compactly supported wavelets: *Communications on Pure and Applied Mathematics*, **41**, 909–996, doi: [10.1002/\(ISSN\)1097-0312](https://doi.org/10.1002/(ISSN)1097-0312).
- Daubechies, I., 1992, Ten lectures on wavelets: SIAM, CBMS-NSF Regional Conference Series in Applied Mathematics.
- Daubechies, I., J. F. Lu, and H. T. Wu, 2011, Synchrosqueezed wavelet transforms: An empirical mode decomposition-like tool: *Applied and Computational Harmonic Analysis*, **30**, 30243–30261.
- Donoho, D., 1995, Nonlinear solution of linear inverse problems by wavelet-vaguelette decomposition, *Applied Computational and Harmonic Analysis*, **2**, 101–126.
- Daubechies, I., and S. Maes, 1996, A nonlinear squeezing of the continuous wavelet transform based on auditory nerve models: *Wavelets in Medicine and Biology*, 527–546.
- Donoho, D., and I. M. Johnstone, 1994, Ideal spatial adaptation by wavelet shrinkage: *Biometrika*, **81**, 425–455, doi: [10.1093/biomet/81.3.425](https://doi.org/10.1093/biomet/81.3.425).
- Duncan, P. M., and L. Eisner, 2010, Reservoir characterization using surface microseismic monitoring: *Geophysics*, **75**, no. 5, 75A139–75A146, doi: [10.1190/1.3467760](https://doi.org/10.1190/1.3467760).
- Earle, P. S., and P. M. Shearer, 1994, Characterization of global seismograms using an automatic-picking algorithm: *Bulletin of Seismological Society of America*, **84**, 366–376.

- Eaton, D., M. van der Baan, J. B. Tary, B. Birkelo, N. Spriggs, S. Cutten, and K. Pike, 2013, Broadband microseismic observations from a Montney hydraulic fracture treatment, northeastern British Columbia: CSEG Recorder, **38**, 45–53.
- Eisner, L., D. Abbott, W. Barker, J. Lakings, and M. Thornton, 2008, Noise suppression for detection and location of microseismic events using a matched filter: 78th Annual International Meeting, SEG, Expanded Abstracts, 1431–1435.
- Eisner, L., V. Grechka, and S. Williams-Stroud, 2010, Future of microseismic analysis: Integration of monitoring and reservoir simulation: Hedberg Conference, AAPG, Abstract, Search and Discovery articles #90122.
- Eisner, L., B. J. Hulsey, P. Duncan, D. Jurick, and H. Werner, 2009, Comparison of surface and borehole locations of induced seismicity: Geophysical Prospecting, **176**, 31–39, doi: [10.1111/j.1365-2478.2010.00867.x](https://doi.org/10.1111/j.1365-2478.2010.00867.x).
- Farge, M., 1992, Wavelet transforms and their applications to turbulence: Annual Review of Fluid Mechanics, **24**, 395–458, doi: [10.1146/annurev.fl.24.010192.002143](https://doi.org/10.1146/annurev.fl.24.010192.002143).
- Galiana-Merino, J. J., J. Rosa-Herranz, and S. Parolai, 2008, Seismic P phase picking using a Kurtosis-based criterion in the stationary wavelet domain: IEEE Transaction on Geoscience and Remote Sensing, **46**, 3815–3826, doi: [10.1109/TGRS.2008.2002647](https://doi.org/10.1109/TGRS.2008.2002647).
- Gentili, S., and A. Michelini, 2006, Automatic picking of P- and S-phases using a neural tree: Journal of Seismology, **10**, 39–63, doi: [10.1007/s10950-006-2296-6](https://doi.org/10.1007/s10950-006-2296-6).
- Gibbons, S. J., and F. Ringdal, 2006, The detection of low magnitude seismic events using array-based waveform correlation: Geophysical Journal International, **165**, 149–166, doi: [10.1111/gji.2006.165.issue-1](https://doi.org/10.1111/gji.2006.165.issue-1).
- Grossmann, A., and J. Morlet, 1984, Decomposition of hardy functions into square integrable, wavelets of constant shape: SIAM Journal on Mathematical Analysis, **15**, 723–736, doi: [10.1137/0515056](https://doi.org/10.1137/0515056).
- Han, J., and M. van der Baan, 2015, Microseismic and seismic denoising via ensemble empirical mode decomposition and adaptive thresholding: Geophysics, **80**, no. 6, KS69–KS80, doi: [10.1190/geo2014-0423.1](https://doi.org/10.1190/geo2014-0423.1).
- Heil, C. E., and D. F. Walnut, 1989, Continuous and discrete wavelet transforms: SIAM Review, **31**, 628–666, doi: [10.1137/1031129](https://doi.org/10.1137/1031129).
- Herrera, R. H., J. Han, and M. van der Baan, 2014, Applications of the synchrosqueezing transform in seismic time-frequency analysis: Geophysics, **79**, no. 3, V55–V64, doi: [10.1190/geo2013-0204.1](https://doi.org/10.1190/geo2013-0204.1).
- Herrera, R. H., M. van der Baan, and D. W. Eaton, 2015, Body wave separation in the time-frequency domain: IEEE Geoscience Remote Sensing Letters, **12**, 364–368, doi: [10.1109/LGRS.2014.2342033](https://doi.org/10.1109/LGRS.2014.2342033).
- Jurkevicius, A., 1988, Polarization analysis of three component array data: Bulletin of Seismological Society of America, **78**, 1725–1743.
- Kanasewich, E. R., 1981, Time sequence analysis in geophysics: University of Alberta Press.
- Karamzadeh, N., G. J. Doloei, and A. Reza, 2013, Automatic earthquake signal onset picking based on the continuous wavelet transform: IEEE Transaction on Geoscience and Remote Sensing, **51**, 2666–2674, doi: [10.1109/TGRS.2012.2213824](https://doi.org/10.1109/TGRS.2012.2213824).
- Küperkoch, L., T. Meier, J. Lee, and W. Friederich, and , Working Group EGELEADOS, 2010, Automated determination of P-phase arrival times at regional and local distances using higher order statistics: Geophysical Journal International, **181**, 1159–1170, doi: [10.1111/j.1365-246X.2010.04570.x](https://doi.org/10.1111/j.1365-246X.2010.04570.x).
- Leonard, M., 2000, Comparison of manual and automatic onset time picking: Bulletin of Seismological Society of America, **90**, 1384–1390, doi: [10.1785/0120000026](https://doi.org/10.1785/0120000026).
- Leonard, M., and B. L. N. Kennet, 1999, Multi-component autoregressive techniques for the analysis of seismograms: Physics of the Earth and Planetary Interiors, **113**, 247–263, doi: [10.1016/S0031-9201\(99\)0054-0](https://doi.org/10.1016/S0031-9201(99)0054-0).
- Li, C., and M. Liang, 2012, A generalized synchrosqueezing transform for enhancing signal time-frequency representation: Signal Processing, **92**, 2264–2274, doi: [10.1016/j.sigpro.2012.02.019](https://doi.org/10.1016/j.sigpro.2012.02.019).
- Lois, A., E. Sokos, N. Martakis, P. Paraskevopoulos, and G. A. Tselentis, 2013, A new automatic S-onset detection technique: Application in local earthquake data: Geophysics, **78**, no. 1, KS1–KS11, doi: [10.1190/geo2012-0050.1](https://doi.org/10.1190/geo2012-0050.1).
- Maeda, N., 1985, A method for reading and checking phase times in auto-processing system of seismic wave data: Journal of the Seismological Society of Japan, **38**, 365–379.
- Magotra, N., N. Ahmed, and E. Chael, 1989, Single-station seismic event detection and location: IEEE Transaction on Geoscience and Remote Sensing, **27**, 15–23, doi: [10.1109/36.20270](https://doi.org/10.1109/36.20270).
- Magotra, N., N. Ahmed, and E. Chael, 1987, Seismic event detection and source location using single-station (three-component) data: Bulletin of Seismological Society of America, **77**, 958–971.
- Mallat, S., 1999, A wavelet tour of signal processing, in wavelet analysis and its applications (2nd ed.): Academic Press, 620.
- Maxwell, S. C., 2005, A brief guide to passive seismic monitoring: Proceedings of the CSEG National Convention, 177–178.
- Maxwell, S. C., J. Shemeta, E. Campbell, and D. Quirk, 2008, Microseismic deformation rate monitoring: Annual Technical Conference and Exhibition, Society of Petroleum Engineers, SPE 11659.
- McLachlan, G., and D. Peel, 2000, Finite mixture models: Wiley.
- McNamara, D. E., and R. P. Buland, 2004, Ambient noise levels in the continental united states: Bulletin of the Seismological Society of America, **94**, 1517–1527, doi: [10.1785/012003001](https://doi.org/10.1785/012003001).
- McNamara, D. E., M. Meremonte, J. Z. Maharrey, S.-L. Mildore, J. R. Altidore, D. Anglade, S. E. Hough, D. Given, H. Benz, L. Gee, and A. Frankel, 2012, Frequency-dependent seismic attenuation within the Hispaniola Island region of the Caribbean sea: Bulletin of the Seismological Society of America, **102**, 773–782, doi: [10.1785/0120110137](https://doi.org/10.1785/0120110137).
- Mendecki, A. J., 1993, Real time quantitative seismology in mines: Keynote address: Proceedings of the 3rd International Symposium on Rockbursts and Seismicity in Mines, 287–295.
- Mousavi, S. M., C. H. Cramer, and C. A. Langston, 2014, Average QLg, QSn, and observation of Lg blockage in the continental margin of Nova Scotia: Journal of Geophysical Research, **119**, 7722–7744, doi: [10.1002/2014JB011237](https://doi.org/10.1002/2014JB011237).
- Mousavi, S. M., S. P. Horton, and C. A. Langston, 2015, Exploring differences between epicenter locations from an array of surface seismometers and a downhole array of geophones: Proceedings of the SSA Annual Meeting.
- Mousavi, S. M., and C. A. Langston, 2016, Hybrid seismic denoising using higher-order statistics and improved wavelet block thresholding: Bulletin of Seismological Society of America, **106**, doi: [10.1785/0120150345](https://doi.org/10.1785/0120150345).
- Mousset, E., Y. Cansi, R. Crusem, and Y. Souchet, 1996, A connectionist approach for automatic labeling of regional seismic phases using a single vertical component seismogram: Geophysical Research Letters, **23**, 681–684, doi: [10.1029/95GL03811](https://doi.org/10.1029/95GL03811).
- Naghizadeh, M., 2011, Seismic data interpolation and denoising in the frequency-wavenumber domain: Geophysics, **77**, no. 2, V71–V80, doi: [10.1190/geo2011-0172.1](https://doi.org/10.1190/geo2011-0172.1).
- Naghizadeh, M., and M. Sacchi, 2012, Multicomponent f-x seismic random noise attenuation via vector autoregressive operators: Geophysics, **77**, no. 2, V91–V99, doi: [10.1190/geo2011-0198.1](https://doi.org/10.1190/geo2011-0198.1).
- Nippes, S. E. J., A. Rietbroek, and A. E. Heath, 2010, Optimized automatic pickers: Application to the ANCORP data set: Geophysical Journal International, **181**, 911–925, doi: [10.1111/j.1365-246X.2010.04531.x](https://doi.org/10.1111/j.1365-246X.2010.04531.x).
- Otsu, N., 1979, A threshold selection method from gray-level histograms: IEEE Transaction on Systems, Man and Cybernetics, **9**, 62–66, doi: [10.1109/TSMC.1979.4310076](https://doi.org/10.1109/TSMC.1979.4310076).
- Panagiotakis, C., E. Kokinou, and F. Vallianatos, 2008, Automatic P-phase picking based on local-maxima distribution: IEEE Transaction on Geoscience and Remote Sensing, **46**, 2280–2287, doi: [10.1109/TGRS.2008.917272](https://doi.org/10.1109/TGRS.2008.917272).
- Parolai, S., 2009, Denoising of seismograms using the S transform: Bulletin of Seismological Society of America, **99**, 226–234, doi: [10.1785/0120080001](https://doi.org/10.1785/0120080001).
- Pearson, C., 1981, The relationship between microseismicity and high pore pressures during hydraulic stimulation experiments in low permeability granitic rocks: Journal of Geophysical Research, Solid Earth, **86**, 7855–7864, doi: [10.1029/JB086iB09p07855](https://doi.org/10.1029/JB086iB09p07855).
- Pettitt, W., J. Reyes-montes, B. Hemmings, E. Hughes, and R. P. Young, 2009, Using continuous microseismic records for hydrofracture diagnostics and mechanics: 79th Annual International Meeting, SEG, Expanded Abstracts, 1542–1546.
- Poletto, F., 2000, A blind interpretation of drill-bit signals: Geophysics, **65**, 970–978, doi: [10.1190/1.1444793](https://doi.org/10.1190/1.1444793).
- Robert, R. G., A. Christoffersson, and F. Cassidy, 1989, Real-time event detection, phase identification and source location estimation using single station three-component seismic data: Geophysical Journal International, **97**, 471–480, doi: [10.1111/gji.1989.97.issue-3](https://doi.org/10.1111/gji.1989.97.issue-3).
- Rosca, A., and C. Maisons, 2012, Validation of surface and shallow microseismic array for deep reservoir monitoring: SPE/EAGE European Unconventional Resources Conference and Exhibition, 153035, doi: [10.2118/153035-MS](https://doi.org/10.2118/153035-MS).
- Ross, Z. E., and Y. Ben-Zion, 2014, Automatic picking of direct P, S seismic phases and fault zone head waves: Geophysical Journal International, **199**, 368–381, doi: [10.1093/gji/ggu267](https://doi.org/10.1093/gji/ggu267).
- Ruud, B. O., and E. S. Husebye, 1992, A new three-component detector and automatic single-station bulletin production: Bulletin of Seismological Society of America, **82**, 221–237.
- Saari, J., 1991, Automated phase picker and source location algorithm for local distances using a single three-component seismic station: Tectonophysics, **189**, 307–315, doi: [10.1016/0040-1951\(91\)90503-K](https://doi.org/10.1016/0040-1951(91)90503-K).
- Saragiots, C. D., L. J. Hadjileontiadis, and S. M. Panas, 1999, A higher-order statistics-based phase identification of three-component seismograms in a redundant wavelet transform domain: Proceedings of IEEE Workshop High-Order Statistic, 396–399.
- Saragiots, C. D., L. J. Hadjileontiadis, and S. M. Panas, 2002, PAI-S/K: A robust automatic seismic P phase arrival identification scheme: IEEE

- Transaction on Geoscience and Remote Sensing, **40**, 1395–1404, doi: [10.1109/TGRS.2002.800438](https://doi.org/10.1109/TGRS.2002.800438).
- Saragiotsis, C. D., L. J. Hadjileontiadis, I. T. Rekanos, and S. M. Panas, 2004, Automatic P phase picking using maximum kurtosis and k-statistics criteria: IEEE Transaction on Geoscience and Remote Sensing Letters, **1**, 147–151, doi: [10.1109/LGRS.2004.828915](https://doi.org/10.1109/LGRS.2004.828915).
- Shemeta, J., and P. Anderson, 2010, It's a matter of size: Magnitude and moment estimates for microseismic data: The Leading Edge, **29**, 296–302, doi: [10.1190/1.3353726](https://doi.org/10.1190/1.3353726).
- Simons, F. J., B. D. E. Dando, and R. M. Allen, 2006, Automatic detection and rapid determination of earthquake magnitude by wavelet multiscale analysis of the primary arrival: Earth and Planetary Science Letters, **250**, 214–223, doi: [10.1016/j.epsl.2006.07.039](https://doi.org/10.1016/j.epsl.2006.07.039).
- Simpson, D., W. Leith, and C. Scholz, 1988, Two types of reservoir-induced seismicity: Bulletin of Seismological Society of America, **78**, 2025–2040.
- Sobolev, G., and A. Lyubushin, 2006, Microseismic impulses as earthquake precursors: Izvestiya: Physics of the Solid Earth, **42**, 721–733, doi: [10.1134/S1069351306090023](https://doi.org/10.1134/S1069351306090023).
- Sleeman, R., and T. Van Eck, 1999, Robust automatic P-phase picking: An on-line implementation in the analysis of broadband seismogram recordings: Physics of the Earth and Planetary Interiors, **113**, 265–275, doi: [10.1016/S0031-9201\(99\)00007-2](https://doi.org/10.1016/S0031-9201(99)00007-2).
- Tary, J. B., R. H. Herrera, and M. van der Baan, 2013, Time-varying autoregressive model for spectral analysis of microseismic experiments and long-period volcanic events: Geophysical Journal International, **196**, 600–611, doi: [10.1093/gji/gjt400](https://doi.org/10.1093/gji/gjt400).
- Tary, J. B., R. H. Herrera, J. Han, and M. van der Baan, 2014, Spectral estimation — What is new? What is next?: Reviews of Geophysics, **52**, 723–749, doi: [10.1002/2014RG000461](https://doi.org/10.1002/2014RG000461).
- Tary, J. B., and M. van der Baan, 2012, Potential use of resonance frequencies in microseismic interpretation: The Leading Edge, **31**, 1338–1346, doi: [10.1190/tle31111338.1](https://doi.org/10.1190/tle31111338.1).
- Taylor, K. M., M. J. Procopio, C. J. Young, and F. G. Meyer, 2011, Estimation of arrival times from seismic waves: A manifold-based approach: Geophysical Journal International, **185**, 435–452, doi: [10.1111/gji.2011.185.issue-1](https://doi.org/10.1111/gji.2011.185.issue-1).
- Thakur, G., E. Brevdo, N. S. Fuckar, and H. T. Wu, 2013, The synchrosqueezing algorithm for time-varying spectral analysis: Robustness properties and new paleoclimate applications: Signal Processing, **93**, 1079–1094, doi: [10.1016/j.sigpro.2012.11.029](https://doi.org/10.1016/j.sigpro.2012.11.029).
- Tselentis, G. A., N. Martakis, P. Paraskevopoulos, A. Lois, and E. Sokos, 2012, Strategy for automated analysis of passive microseismic data based on S-transform, Otsu's thresholding, and higher order statistics: Geophysics, **77**, no. 6, KS43–KS54, doi: [10.1190/geo2011-0301.1](https://doi.org/10.1190/geo2011-0301.1).
- Vidale, J. E., 1986, Complex polarization analysis of particle motion: Bulletin of Seismological Society of America, **76**, 1393–1405.
- Wagenmakers, E. J., and S. Farrell, 2004, AIC model selection using Akaike weights: Psychonomic Bulletin and Review, **11**, 192–196, doi: [10.3758/BF03206482](https://doi.org/10.3758/BF03206482).
- Wang, J., and T. Teng, 1995, Artificial neural network-based seismic detector: Bulletin of Seismological Society of America, **85**, 308–319.
- Withers, M., R. Aster, C. Young, J. Beiriger, M. Harris, S. Moore, and J. Trujillo, 1998, A comparison of select trigger algorithms for automated global seismic phase and event detection: Bulletin of Seismological Society of America, **88**, 95–106.
- Wu, H. T., P. Flandrin, and I. Daubechies, 2011, One or two frequencies? The synchrosqueezing answers: Advances in Adaptive Data Analysis, **3**, 29–39, doi: [10.1142/S179353691100074X](https://doi.org/10.1142/S179353691100074X).
- Yang, H., 2015, Synchrosqueezing wave packet transforms and diffeomorphism based spectral analysis for 1D general mode decompositions: Applied and Computational Harmonic Analysis, **39**, 33–66, doi: [10.1016/j.acha.2014.08.004](https://doi.org/10.1016/j.acha.2014.08.004).
- Yoon, B. J., and P. P. Vaidyanathan, 2004, Wavelet-based denoising by customized thresholding: IEEE International Conference on Acoustic Speech and Signal Processing (ICASSP), 925–928.
- Yung, S. K., and L. T. Ikelle, 1997, An example of seismic time picking by 3rd order bicoherence: Geophysics, **62**, 1947–1952, doi: [10.1190/1.1444295](https://doi.org/10.1190/1.1444295).
- Zhang, H., C. Thurber, and C. Rowe, 2003, Automatic P-wave arrival detection and picking with multiscale wavelet analysis for single-component recordings: Bulletin of Seismological Society of America, **93**, 1904–1912, doi: [10.1785/0120020241](https://doi.org/10.1785/0120020241).
- Zhao, Y., and K. Takano, 1999, An artificial neural network-based seismic detector: Bulletin of Seismological Society of America, **77**, 670–680.
- Zoback, M. D., A. Kohli, I. Das, and M. McClure, 2012, The importance of slow slip on faults during hydraulic fracturing stimulation of shale gas reservoirs: Presented at the Americas Unconventional Resources Conference, SPE, Paper 155476.